Available online at www.sciencedirect.com
SCIENCE DIRECT
Journal of Molecular Catalysis A: Chemical 244 (2006) 25–32
JOURNAL OF MOLECULAR CATALYSIS A: CHEMICAL
www.elsevier.com/locate/molcata

Characterization and photocatalytic mechanism of nanosized CdS coupled TiO_2 nanocrystals under visible light irradiation

Ling Wu [a,b,*], Jimmy C. Yu [b], Xianzhi Fu [a]

[a] *Research Institute of Photocatalysis, Fuzhou University, Fuzhou, Fujian 350002, China*
[b] *Department of Chemistry, The Chinese University of Hong Kong, Shatin, New Territories, Hong Kong*

Received 24 May 2005; received in revised form 9 August 2005; accepted 30 August 2005
Available online 3 October 2005

Abstract

Nanosized CdS coupled TiO_2 nanocrystals were prepared by a microemulsion-mediated solvothermal method at relatively low temperatures. The prepared samples were characterized by X-ray photoelectron spectroscopy (XPS), BET surface area analysis, X-ray diffraction (XRD), UV–vis absorption spectroscopy (UV–vis), transmission electron microscopy (TEM) and high-resolution transmission electron microscopy (HRTEM). It was found that the CdS coupled TiO_2 materials consisted of uniform anatase TiO_2 of 6–10 nm with highly dispersed cubic phase CdS nanocrystals. The prepared samples exhibit strong visible light absorption at about 550 nm. Meanwhile, they have high surface area in the range of 156–263 $m^2\ g^{-1}$ and mesoporous character with the average pore diameter of ca. 5.0–6.5 nm. The coupling between the (1 0 1) crystal planes of anatase and (1 1 1) crystal planes of CdS was observed in the HRTEM image. Ti^{3+} signal was observed in the electron paramagnetic resonance (EPR) spectrum of CdS coupled TiO_2 nanocrystals under visible light irradiation. It provided the evidence of an effective transfer of photo-generated electrons from the conduction band of CdS to that of TiO_2. As expected, the nanosized CdS sensitized TiO_2 nanocrystal materials showed enhanced activity in the oxidation of methylene blue in water or nitric oxide in air under visible light irradiation. The mechanism of photocatalysis on CdS coupled TiO_2 nanocrystals under visible light is also discussed.

Keywords: Nanosized; CdS coupled TiO_2; Visible light; Electron transfer; Photocatalytic activity

1. Introduction

TiO_2 is the most widely used photocatalyst for effective decomposition of organic compounds in air and water under irradiation of UV light with wavelength shorter than that corresponding to its band gap energy [1–10]. However, only about 3–5% of the solar spectrum falls in this UV range. This limits the efficient utilization of solar energy for TiO_2. The efficient use of sunlight has thus become an appealing challenge for developing photocatalytic technologies [11–14]. To improve the response of TiO_2 to visible light, transition metal [15–20] or non-metal atom [21–27] doped TiO_2 and dye [28–32] or metal complex [33–36] sensitized TiO_2 have been developed. Alternative approach for achieving this objective is to couple TiO_2 by using a narrow band gap semiconductor with a higher conduction band (CB) than that of TiO_2. In this sensitized TiO_2, charge injection from the CB of the narrow band gap semiconductor to that of TiO_2 can lead to efficient and longer charge separation by minimizing the electron–hole recombination. For instance, CdS coupled TiO_2 colloids have been extensively studied in photoelectrochemistry and water splitting systems [37–44]. However, only bulk CdS mixed TiO_2 particles were developed for visible light photocatalysis [45]. The bulk nature may decrease the coupled ability of CdS. Utilization of nanosized CdS to couple nanocrystalline TiO_2 could improve its photocatalytic efficiency due to their high surface area and high dispersibility in a solution.

It would be desirable to directly prepare TiO_2 nanocrystalline particles with homogeneously dispersed CdS nanocrystals, because the direct formation of these two semiconductors would provide a strong coupling between them. Therefore, we developed a new approach to facilitate the direct formation of nanocrystalline TiO_2 coupled by highly dispersed CdS nanocrystals at a considerably lower temperature by a combined

* Corresponding author. Tel.: +86 591 83731234 8507; fax: +86 591 83773729.
E-mail address: wwuljh83@yahoo.com.cn (L. Wu).

1381-1169/$ – see front matter © 2005 Elsevier B.V. All rights reserved.
doi:10.1016/j.molcata.2005.08.047

microemulsion and solvothermal method [46]. This method can prevent the oxidation of CdS in CdS/TiO_2 nanocomposite during thermal treatment for the crystallization of TiO_2 [47]. A microemulsion is thermodynamically stable, commonly consisting of two immiscible components (aqueous and oil phases) and a surfactant [48,49]. In a water-in-oil microemulsion, water is highly dispersed in oil phase (continuous phase) as nanodroplets stabilized by a monolayer of interfacial surfactant film. These tiny water droplets in the oil phase can be used as chemical reactors for the synthesis of nanoparticles. Therefore, water-in-oil microemulsions have been used as microreactors to prepare monodispersed nanoparticles and to control particle size and crystal structure by adjusting concentrations of reactants, pH values, reactive temperature and so on [50–52]. On the other hand, a solvothermal method is very useful in the synthesis of versatile inorganic materials. The advantageous aspects of the solvothermal synthesis route are the formation of homogeneous samples of complex mixed-metal solids, the control of crystal form and the isolation of metastable phases in low temperature [53,54].

Here, we in detail report synthesis, characterization and visible light photocatalysis of the nanosized CdS coupled TiO_2 nanocrystal (CdS/TiO_2) photocatalysts. The experiment results clearly give the evidence of an effective transfer of photogenerated electrons from the conduction band of CdS to that of TiO_2 and also show well coupling between TiO_2 and CdS. Meanwhile, photocatalytic active evaluations show that the samples have high activity on the oxidation of both methylene blue in water and nitric oxide in air under visible light irradiation. The mechanism of photocatalysis on CdS/TiO_2 under visible light is also discussed.

2. Experimental

2.1. Synthesis

Titanium tetraisopropoxide (TTIP) was used as a titanium source. $Cd(NO_3)_2$ and $(NH_4)_2S$ were used as precursors of CdS. A typical synthesis of sample S2 (CdS at 3%) involved the use of cyclohexane (0.9 mol) as oil phase, Triton X-100 (0.028 mol) as surfactant and 1-hexanol (0.056 mol) as co-surfactant. Three microemulsions containing 1 mL of Millipore water (A), 1.5 mL of 0.3 M $Cd(NO_3)_2$ solution (B) and 2.5 mL of 20 wt% $(NH_4)_2S$ solution (C) were prepared. Titanium isopropoxide (14.55 mmol) was added into microemulsion (A) under continuous stirring. After titanium isopropoxide was gradually hydrolyzed and condensed in water nanodroplets for 30 min, microemulsion B was mixed with microemulsion A under vigorous agitation. Microemulsion C was then added into the mixture. This new microemulsion was stirred for 24 h at room temperature. In this process, cadmium sulfide was incorporated into the TiO_2 colloids by simultaneous coprecipitation of $Cd(NO_3)_2$ and $(NH_4)_2S$ in the water nanodroplets. Seventy five millilitres of the resulting microemulsion colloids containing CdS and TiO_2 was placed in a 100 mL Teflon-lined stainless steel autoclave and bubbled with Ar gas to remove air from the colloids, then solvothermally treated at 200 °C for 12 h. The yellow slurry obtained was centrifuged and washed with ethanol and water before finally being kept in a desiccator for drying. Samples S1 and S3 (CdS at 1 and 5 mol% nominal values, respectively), pure TiO_2 and CdS were also synthesized by similar procedures.

2.2. Characterization

X-ray photoelectron spectroscopy (XPS) measurements were done with a PHI Quantum 2000 XPS System with a monochromatic Al Kα source and a charge neutralizer; all the binding energies were referenced to the C 1s peak at 284.8 eV of the surface adventitious carbon. The Brunauer–Emmett–Teller (BET) surface area (S_{BET}) and pore size distribution were determined using a Micromeritics ASAP 2010 nitrogen adsorption apparatus. All the samples were degassed at 180 °C prior to BET measurements. UV–vis absorption spectra were recorded on a Varian Cary 100 Scan UV–vis system equipped with a labsphere diffuse reflectance accessory. XRD patterns were obtained on a Bruker D8 Advance X-ray diffractometer with Cu Kα radiation at a scan rate of $0.02^\circ\ 2\theta\ S^{-1}$. The accelerating voltage and the applied current were 40 kV and 40 mA, respectively. The crystallite size was calculated from X-ray line broadening by the Scherrer equation: $D = 0.89\lambda/\beta \cos\theta$, where D is the crystal size in nm, λ the Cu Kα wavelength (0.15406), β the half-width of the peak in radians and θ is the corresponding diffraction angle. TEM and HRTEM images were taken on a Philips CM-120 electron microscopy instrument and a JEOL2010 transmission electron microscopy instrument at an accelerating voltage of 200 kV, respectively. A suspension in ethanol was sonicated, and a drop was dropped on the support film. The powder particles were then supported on a carbon film coated on a 3 mm diameter fine-mesh copper grid. EPR spectrum was recorded on an X-band EPR spectrometer (JEOL, JES-TE100) at 77 K. The CdS/TiO_2 sample was placed into a quartz tube, which was evacuated and then refilled with oxygen gas and sealed. The sample was irradiated by a 500 W superhigh-pressure mercury lamp (Ushio, USH500D) equipped with a bandpass filter of 424 nm (Toshiba, Y-44). The settings for the EPR spectrometer were center field, 323.366 mT; sweep width, 25 mT; microwave frequency, 9.075 GHz; power, 449 μW.

2.3. Photocatalytic activity

Visible-light photocatalytic activities of the samples were measured by the decomposition rate of methylene blue in an aqueous solution. Air was bubbled into the solution throughout the entire experiment. A 300 W tungsten halogen lamp was positioned inside a cylindrical Pyrex vessel and surrounded by a circulating water jacket (Pyrex) to cool the lamp. A cut-off filter was placed outside the Pyrex jacket to completely remove all wavelengths less than 400 nm to ensure irradiation with visible light only (light region I: >400 nm). Moreover, a saturated cupric acetate solution as a filter was put in front of a reactor to obtain a light source with a region (II) 400–580 nm. 0.15 g of photocatalyst (pure CdS is 8 mg which is the same amount of CdS present in sample S2) was suspended in a 200 mL aqueous solu-

tion of 2.2×10^{-5} M methylene blue. Prior to irradiation, the suspensions were magnetically stirred in the dark for ca. 40 min to ensure establishment of an adsorption/desorption equilibrium among the photocatalyst, methylene blue and atmospheric oxygen. At given irradiation time intervals, 4 mL of the suspensions were collected, then centrifuged and filtered through a Millipore filter (pore size, 0.22 in.) to separate the photocatalyst particles. The degraded solutions of MB were analyzed by a Varian Cary 100 Scan UV–vis spectrophotometer and the absorption peak at 660 nm was monitored.

The photocatalytic activity of sample S2 was also evaluated by oxidation of NO in an air flow under visible light irradiation. A constant 3 L/min of air mixture containing about 1000 ppb of NO was supplied through the inlet to a gas flow photo-reactor, while the concentration of NO was detected at the outlet of the reactor. 0.3 g of sample S2 as a photocatalyst coated in three Petri dishes was placed in the reactor. A NO_x analyzer was used to measure NO_x concentrations on line. When the NO concentration of the gas flow was steady in the reactor, a lamp was turned on for irradiation. A 300 W tungsten halogen lamp with a 400 nm cut off filter and a 15 W daily fluorescent light lamp were used as light sources though the Pyrex glass window of the reactor to irradiate the photocatalyst.

3. Results and discussion

3.1. Nitrogen adsorption and XPS analysis

Fig. 1 shows pore size distribution curves calculated from the desorption branch of the nitrogen adsorption–desorption isotherms by the Barrett–Joyner–Halenda (BJH) method and the corresponding isotherms (inset) of samples. The sharp decline in desorption curves and the isotherms of type IV with H4 hysteresis-loop are indicative of mesoporosity [55,56]. The pore size distributions exhibit the narrow range of 2.0–11.0 nm with the average pore diameter of ca. 5.0–6.5 nm. Table 1 shows that the samples have high surface area in the range of 156–263 $m^2\ g^{-1}$ and single point total pore volume in the range

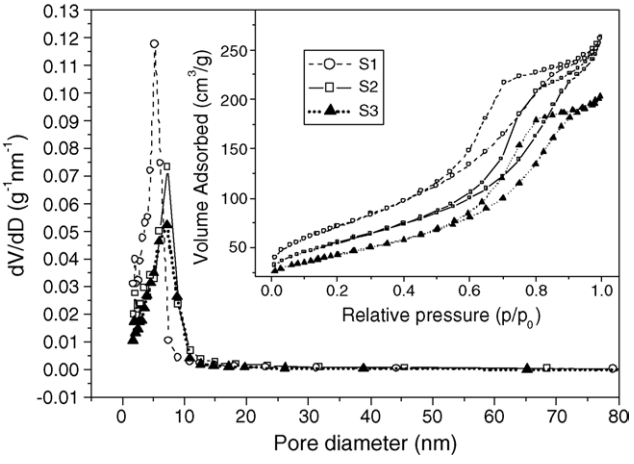

Fig. 1. N_2 adsorption–desorption isotherms (inset) and BJH pore size distributions: (◯) sample S1, (□) sample S2, (▲) sample S3.

Table 1
Summary of the physicochemical properties of the samples

Sample	CdS (mol%)		S_{BET}[c] ($m^2\ g^{-1}$)	Mean pore size[d] (nm)	Total pore volume[e] ($cm^{-3}\ g^{-1}$)	Crystal size[f] (nm)
	N_1[a]	N_2[b]				
S1	1	1.07	263	5	0.38	5.6
S2	3	2.8	201	6.5	0.37	8.8
S3	5	5.36	156	6	0.30	9.8

[a] Nominal value.
[b] Measured by XPS.
[c] BET surface area calculated from the linear part of the BET plot.
[d] Estimated using the BJH desorption branch of the isotherm.
[e] Single point total pore volume of pores at $P/P_0 = 0.97$.
[f] Calculated by the Scherrer equation.

of 0.30–0.38 $cm^{-3}\ g^{-1}$. From Table 1, it is obviously observed that the surface area, average pore diameter and total pore volume decrease with the increase of CdS amount in the samples. This may be caused by more CdS particles covered TiO_2 surface and larger particle size.

The X-ray photoelectron spectroscopy (XPS) was carried out to determine the chemical composition of the prepared samples and the valence states of various species present therein [57]. As shown in Table 1, CdS was successfully dispersed into TiO_2 at 1.07, 2.80 and 5.36 mol% for samples S1, S2 and S3, respectively. Fig. 2 shows high-resolution XPS spectra of the four elements of sample S2. The spin–orbit components ($2p_{3/2}$ and $2p_{1/2}$) of the Ti 2p peak were well deconvoluted by two curves at approximately 459.2 and 464.9 eV, corresponding to Ti^{4+} in a tetragonal structure (Fig. 2a). Also, the full width at half maximum (FWHM) of the Ti $2p_{3/2}$ peak is equal to 1.02 eV, consistent with that of TiO_2 powders [58,59]. Similarly, the O 1s XPS spectrum (Fig. 2b) shows a narrow peak with a binding energy of 530.4 eV (FWHM = 1.2 eV) and slight asymmetry. This peak was attributed to the Ti–O in TiO_2 and H_2O or OH groups on the surface of the sample [60,61]. The Cd $3d_{5/2}$ and Cd $3d_{3/2}$ peaks are centered at 405.4 and 412.1 eV with a spin–orbit separation of 6.7 eV, and FWHM of the Cd $3d_{5/2}$ peak equal to 1.16 eV (Fig. 2c). These peaks can be assigned to Cd^{2+} of CdS [57]. The S 2p peak was observed at 161.9 eV (Fig. 2d), corresponding to S^{2-} of CdS nanoparticles [57,62,63].

3.2. XRD analysis and TEM images

X-ray diffraction (XRD) patterns of the prepared CdS/TiO_2 samples were shown in Fig. 3. The five distinctive TiO_2 peaks are found at 25.43°, 37.92°, 48.09°, 54.58°, 62.81° corresponding to the anatase (1 0 1), (1 0 3, 0 0 4 and 1 1 2), (2 0 0), (1 0 5 and 2 1 1), (2 0 4) crystal planes (JCPDS 21-1272), respectively. Meanwhile, the additional peaks at 26.5°, 30.6°, 43.9°, 52.1° were also observed in Fig. 3a and b, which can be assigned to the CdS cubic phase (1 1 1), (2 0 0), (2 2 0) and (3 1 1) crystal planes (JCPDS 89-0440), respectively. No extra peaks except for TiO_2 anatase were observed in Fig. 3c. This may be due to the small amount of CdS in sample S1. Fig. 3a and b also show that the peak intensity of cubic phase CdS increased with an increase in the amount of CdS in the samples. Other phases of

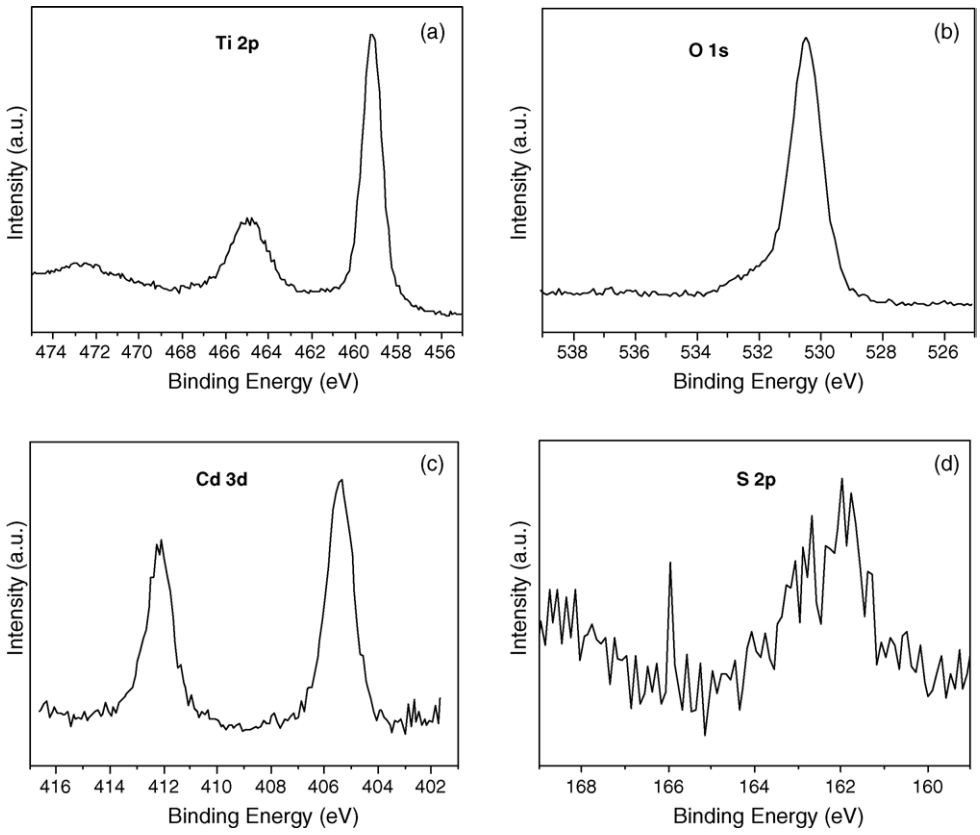

Fig. 2. High-resolution XPS spectra of sample S2: (a) titanium, (b) oxygen, (c) cadmium and (d) sulfur.

TiO_2 and CdS were not observed in the XRD patterns of the prepared samples. The average particle sizes as calculated by the Scherrer formula from (1 0 1) crystal plane of TiO_2 anatase were 5.6, 8.8 and 9.8 nm for samples S1, S2 and S3, respectively. The XRD patterns clearly show that TiO_2 anatase and cubic CdS nanocrystals co-existed in the samples.

A representative TEM image shown in Fig. 4a reveals that nanoparticles in the prepared powder are uniform. Some aggregations among the particles are also observed in Fig. 4a. The average diameter of particles is estimated to be about 8 nm, in agreement with that obtained from XRD. The electron diffraction pattern of sample S2 in the selective area shown in the inset of Fig. 4a indicates that the powders are highly crystalline nanoparticles. No cadmium element was detected by the analysis of EDX. This implies that the coupled cadmium sulfide is highly and homogeneously distributed in the TiO_2 particles. HRTEM examination of sample S2 also reveals the presence of highly crystalline nanoparticles with random orientation and mesopores (Fig. 4c). The fringes appearing in the micrographs allow for the identification of the crystallographic spacing of the TiO_2 and CdS nanocrystallites. The fringes most frequently observed correspond, respectively, to the (1 0 1) crystal planes of TiO_2 anatase. The fringes of $d = 3.7$ and 3.2 Å observed in Fig. 4b match those of the (1 0 1) and (1 1 1) crystal planes of anatase TiO_2 and CdS cubic phase, respectively. The CdS particles being in close contact with TiO_2 particles are easily observed in HRTEM images, indicating the existence of CdS/TiO_2 coupling between the distinct phase domains as well as confirming XPS and XRD results.

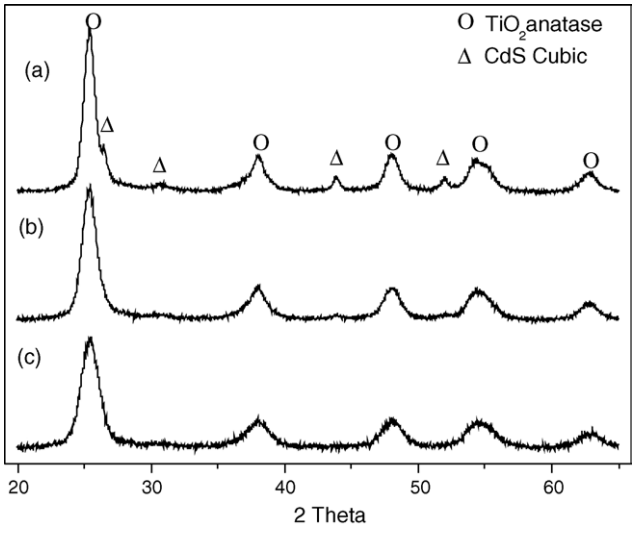

Fig. 3. XRD patterns of the samples: (a) S3, (b) S2, (c) S1 ((◯) anatase TiO_2 and (**Δ**) CdS cubic phase).

3.3. UV–vis diffuse refection spectroscopy

The diffuse reflectance UV–vis absorption spectra of the CdS/TiO_2 samples, pure TiO_2 and CdS are shown in Fig. 5. The CdS/TiO_2 samples exhibit strong absorption peaks in the visible region, while the absorption intensity for the three CdS/TiO_2

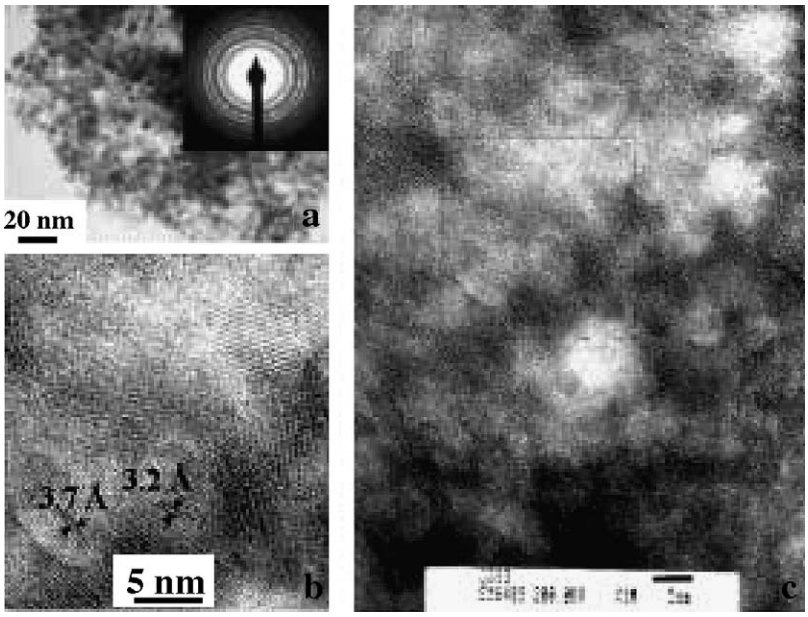

Fig. 4. TEM images of sample S2: (a) TEM image (inset is electron diffraction patterns), (b) HRTEM image of the selective area and (c) HRTEM image.

samples increase with an increasing amount of CdS, in agreement with the progressively intense yellow color of the powders. The absorption onsets were determined by linear extrapolation from the inflection point of the curve to the baseline. The edges of the absorption of the CdS/TiO_2 samples were shifted to approximately 550 nm, corresponding to a band gap energy of 2.25 eV. For comparison, the absorption onsets for anatase TiO_2 and CdS are 410 and 556 nm, corresponding to band gap energies of 3.02 and 2.23 eV, respectively.

3.4. EPR spectroscopy

By comparison of the electron paramagnetic resonance spectrum (EPR) shown in Fig. 6, two obvious signals A and B were produced under visible light irradiation on sample S2 at 77 K in the presence of oxygen in Fig. 6a. Signal B at a g-tensor value of 1.991 can be identified and assigned to the presence of Ti^{3+} on irradiated TiO_2 [64–66]. Meanwhile, no ESR signal of Ti^{3+} could be detected on pure TiO_2. This strongly suggests an effective transfer of photo-generated electrons from the conduction band of CdS to that of TiO_2. Signal A consist of a relatively sharp signal at $g = 2.003$–2.007 and a broad weak signal around $g = 2.029$ in this spectrum. The signal with $g_1 = 2.024$, $g_2 = 2.009$ and $g_3 = 2.003$ was assigned to Ti^{4+}–O_2^- on anatase by some researchers [65–68]. Therefore, we think that signal A in our measurement is produced by O_2^- radical signals on CdS/TiO_2.

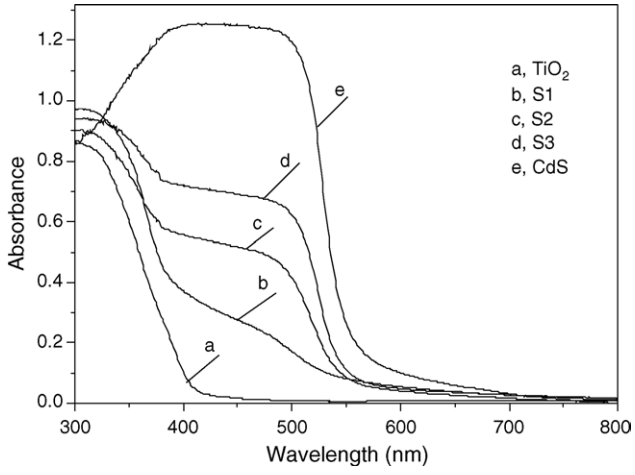

Fig. 5. UV–vis absorption spectra of the samples: (a) TiO_2, (b) sample S1, (c) sample S2, (d) sample S3 and (e) CdS.

3.5. Photocatalytic activity

Photocatalytic activities of the samples were evaluated by measuring the degradation of methylene blue (MB) in aqueous solution under visible light irradiation. Temporal changes in the concentration of MB were monitored by examining the variations in maximal absorption in UV–vis spectra at 660 nm. Fig. 7a shows the results of degradation of MB in the presence of different samples. In the presence of pure TiO_2, degradation of MB was not observed. Similarly, the degradation of MB with pure CdS was not significant. However, in the presence of the CdS/TiO_2 samples, the degradation of MB obviously increased. Among the three CdS/TiO_2 samples, sample S3 exhibited the highest visible light photocatalytic activity. In order to check the self sensitization on MB, we also measured the degradation rate of MB on sample S3 by using light region II (wavelength: 400–580 nm). It was found that the self sensitization of MB was negligible in comparison with CdS sensitization under our experimental conditions.

As shown in Fig. 7b, the absorption peak gradually shifted from 660 to 610 nm with a decrease in absorption during the process of photocatalytic degradation. Such blue-shifted absorption is characteristic of *N*-demethylation derivative(s) of MB. With

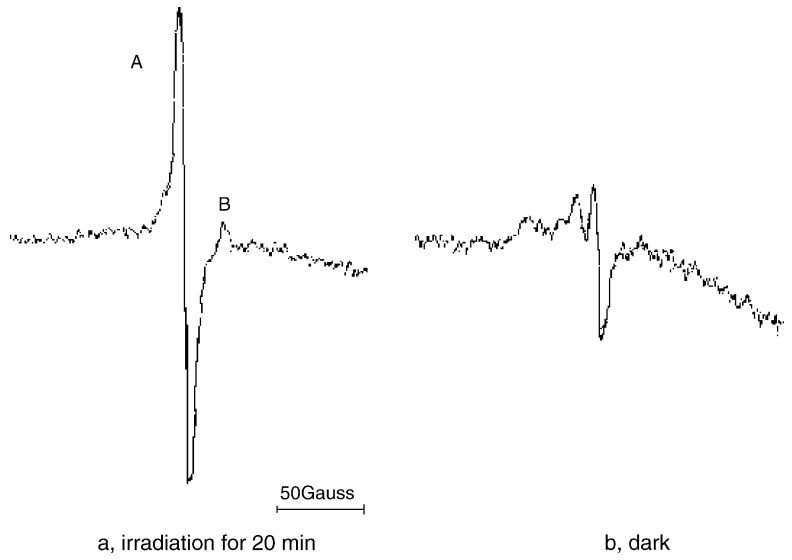

Fig. 6. EPR spectra of sample S2.

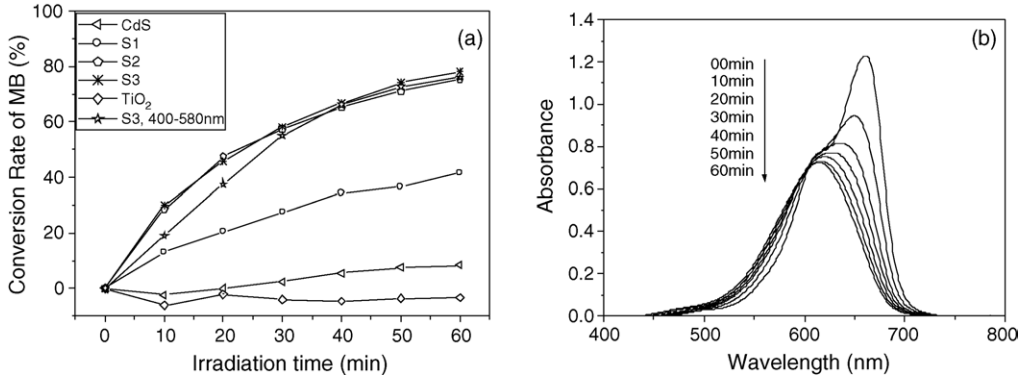

Fig. 7. (a) MB reduction in UV–vis absorption spectra at 660 nm as a function of visible light irradiation time in the prepared photocatalysts. (b) Temporal absorption spectral patterns of MB during the photodegradation process in the sample S2.

the photocatalytic degradation of MB, the absorption peak at 610 nm turned broadened and the absorption peak at 660 disappeared due to the formation of a mixture of *N*-demethylated analogs (Azure B, Azure A, Azure C and Thionine) of MB [69,70]. This result suggested that demethylation process was likely to be a major step in the photocatalytic oxidation of MB.

We also evaluated the photocatalytic activity of sample S2 for the oxidation of NO in air under visible light irradiation. As Fig. 8 shows, under irradiation of both daily fluorescent lamp and UV lamp cut-off 400 nm light, the NO concentration in air flow decreases and the NO removal percentage was about 16–18% for both light sources. NO_2 concentration increases slightly at the initial irradiation stage, then decreases to a constant level. The reason for the initial increase is that the NO_2 is converted to NO^{3-} by reacting with absorbed water accumulated on the catalyst surface [71].

3.6. Mechanism proposal

The interparticle electron transfer between colloid CdS and TiO_2 semiconductor system was investigated [40]. The excited electrons from the CdS particle are quickly transferred to a TiO_2 particle since the conduction band of CdS is −0.5 more negative than that of TiO_2. In our nanosized CdS coupled TiO_2 nanocrystalline system, coupling of two such semiconductor has a beneficial role in improving charge separation and extends

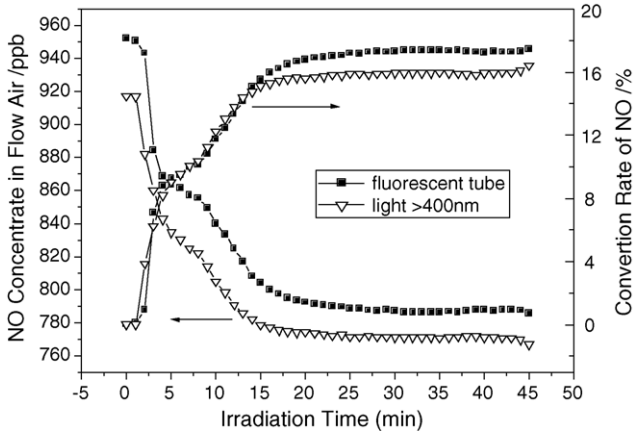

Fig. 8. The decrease of NO concentrate in air flow vs. irradiation time: (■) 300 W tungsten halogen lamp and cut off filter with 400 nm; (▽) 15 W daily fluorescent light.

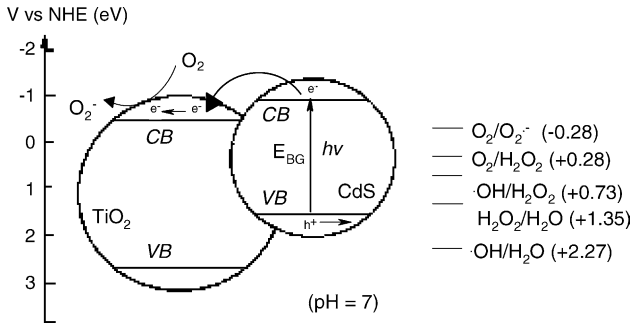

Fig. 9. Redox potentials of the valence and conduction bands of CdS sensitized TiO_2 nanoparticles and various redox processes occurring on their surface at pH 7.

TiO_2 in response to visible light. The ESR result indicates that the electrons from excited CdS are injected into the conduction band of TiO_2 and then scavenged by molecular oxygen O_2 to yield the superoxide radical anion O_2^- in oxygen-equilibrated media. Based on literature reports [4,6,72] and our experiment results, we propose a mechanism for the degradation of pollutants on CdS coupled TiO_2 catalyst under visible light irradiation as shown in Fig. 9. In the system of CdS/TiO_2, anatase TiO_2 can be coupled by interparticle electron transfer from irradiated CdS nanocrystals (Eqs. (1) and (2)) to its conduction band. The electrons are then scavenged by molecular oxygen O_2 to yield the superoxide radical anion O_2^- (Eq. (3)) and hydrogen peroxide H_2O_2 (Eq. (4)) in oxygen-equilibrated media. These new formed intermediates can interreact to produce hydroxyl radical $OH^\bullet$ (Eq. (5)). It is well known that the $OH^\bullet$ radical is a powerful oxidizing agent capable of degrading most pollutants (Eq. (6)) [4,6,73]. This vectorial transfer of charge should therefore enhance the photo-oxidation of the adsorbed organic substrate. However, the photo-generated holes in CdS nanocrystals cannot oxidize hydroxyl groups to hydroxyl radicals due to its valence band potential. This results in the photocorrosion of CdS, forming cadmium cations. An approach is still pursued to make CdS photocatalyst stable.

$$\text{CdS–TiO}_2 \xrightarrow{h\nu} \text{CdS}(e^- + h^+)\text{–TiO}_2 \quad (1)$$

$$\text{CdS}(e^- + h^+)\text{–TiO}_2 \rightarrow \text{CdS}(h^+)\text{–TiO}_2(e^-) \quad (2)$$

$$e^- + O_2 \rightarrow O_2^{-\bullet} \quad (3)$$

$$2e^- + O_2 + 2H^+ \rightarrow H_2O_2 \quad (4)$$

$$H_2O_2 + O_2^{-\bullet} \rightarrow OH^\bullet + OH^- + O_2 \quad (5)$$

$$^\bullet OH + \text{MB} \rightarrow \text{degradation products} \quad (6)$$

4. Conclusions

The experiment results clearly demonstrate that nanosized CdS coupled TiO_2 nanocrystal photocatalysts exhibit the strong coupling and effective electron transfers between nanosized CdS and TiO_2 nanocrystal. BET, XPS, XRD, UV–vis and TEM analysis reveals that the high surface area CdS coupled TiO_2 materials consist of uniform anatase TiO_2 of 6–10 nm with highly dispersed cubic phase CdS nanocrystals, which exhibit strong visible light absorption at about 550 nm. The coupling between the (1 0 1) crystal planes of anatase and (1 1 1) crystal planes of CdS is also clearly observed in the HRTEM image. The formation of Ti^{3+}, as observed in ESR spectrum, confirms an effective transfer of photo-generated electrons from the conduction band of CdS to that of TiO_2. The coupled samples exhibit high efficiency for the decomposition of pollutants in water or air under visible light irradiation. The experiment results also reveal *N*-demethylation of MB is a key process for degradation of MB under visible light irradiation.

Acknowledgments

The work was substantially supported by grants from the National Natural Science Foundation of China (No. 20133010) and the Research Grants Council of the Hong Kong Special Administrative Region, China (Project No. 402904). We thank Mr. Tzekin Cheung of the Hong Kong University of Science and Technology for the HRTEM measurements.

References

[1] N. Serpone, E. Pelizzetti (Eds.), Photocatalysis: Fundamentals and Applications, John Wiley & Sons, New York, 1989.
[2] D.F. Ollis, H. Al-Ekabi (Eds.), Photocatalytic Purification and Treatment of Water and Air, Elsevier, Amsterdam, 1993.
[3] A. Fujishima, K. Hashimoto, T. Watanabe (Eds.), Photocatalysis Fundamentals and Applications, first ed., BKC, Tokyo, 1999.
[4] M. Kaneko, I. Okura (Eds.), Photocatalysis, Science and Technology, Springer, 2002.
[5] M.A. Fox, M.T. Dulay, Chem. Rev. 93 (1993) 341.
[6] M.R. Hoffmann, S.T. Martin, W. Choi, D.W. Bahnemann, Chem. Rev. 95 (1995) 69, and references therein.
[7] L. Linsebigler, G. Lu, J.T. Yates Jr., Chem. Rev. 95 (1995) 735.
[8] A. Mills, R.H. Davies, D. Worsley, Chem. Soc. Rev. 22 (1993) 417.
[9] M. Heller, Acc. Chem. Res. 28 (1995) 503.
[10] A. Fujishima, T.N. Rao, D.A. Tryk, J. Photochem. Photobiol. C: Photochem. Rev. 1 (2000) 1.
[11] R. Asahi, T. Morikawa, K. Aoki, Y. Taga, Science 293 (2001) 269.
[12] S. Khan, M. Al-Shahry, W.B. Ingler, Science 297 (2002) 2243.
[13] Z. Zou, J. Ye, K. Sayama, H. Arakawa, Nature 414 (2001) 625.
[14] H. Kisch, W. Macyk, Chemphyschem 3 (2002) 399.
[15] M. Anpo, M. Takeuchi, J. Catal. 216 (2003) 505.
[16] A. Fuerte, M.D. Hernandez-Alonso, A.J. Maira, A. Martinez-Arias, M. Fernandez-Garcia, J.C. Coneasa, J. Soria, Chem. Commun. (2001) 2718.
[17] W. Zhao, C.C. Chen, X.Z. Li, J.C. Zhao, H. Hidaka, N. Serpone, J. Phys. Chem. B 106 (2002) 5022.
[18] H. Kato, A. Kudo, J. Phys. Chem. B 106 (2002) 5029.
[19] M.I. Litter, Appl. Catal. B: Environ. 23 (1999) 89.
[20] M. Iwasaki, M. Hara, H. Kawada, H. Tada, S. Ito, J. Colloid Interface Sci. 224 (2000) 202.
[21] H. Irie, Y. Watanabe, K. Hashimoto, J. Phys. Chem. B 107 (2003) 5483.
[22] S. Sakthivel, H. Kisch, Chemphychem 4 (2003) 487.
[23] S. Yin, Q.W. Zhang, T. Sato, Chem. Lett. 32 (2003) 358.
[24] S. Sakthivel, H. Kisch, Angew. Chem. Int. Ed. 42 (2003) 4908.
[25] T. Umebayashi, T. Yamaki, S. Tanaka, K. Asai, Chem. Lett. 32 (2003) 330.
[26] T. Ohno, T. Mitsui, M. Matsumura, Chem. Lett. 32 (2003) 364.
[27] K. Nukumizu, J. Nunoshige, T. Takata, J.N. Kondo, M. Hara, Chem. Lett. 32 (2003) 196.
[28] F.R. Fan, A.J. Bard, J. Am. Chem. Soc. 101 (1979) 6139.
[29] C. Nasr, K. Vinodgopal, L. Fisher, S. Hotchandani, A.K. Chattopadhyay, P.V. Kamat, J. Phys. Chem. 100 (1996) 8436.

[30] T. Wu, G. Liu, J. Zhao, H. Hidaka, N. Serpone, J. Phys. Chem. B 103 (1999) 4862.
[31] L. Lucarelli, V. Nadtochenko, J. Kiwi, Langmuir 16 (2000) 1102.
[32] M. Stylidi, D.I. Kondarides, X.E. Verykios, Appl. Catal. B: Environ. 47 (2004) 189.
[33] H. Kisch, L. Zang, C. Lange, W.F. Maier, C. Antonis, D. Meissner, Angew. Chem. Int. Ed. 37 (1998) 3034.
[34] L. Zang, C. Lange, W.F. Maier, I. Abraham, S. Storck, H. Kisch, J. Phys. Chem. B 102 (1998) 10765.
[35] L. Zang, W. Macyk, C. Lange, W.F. Maier, C. Antonis, D. Meissner, H. Kisch, Chem. Eur. J. 6 (2000) 379.
[36] Y.M. Cho, W.Y. Choi, C.H. Lee, T. Hyeon, H.I. Lee, Environ. Sci. Technol. 35 (2001) 966.
[37] L. Spanhel, H. Weller, A. Henglein, J. Am. Chem. Soc. 109 (1987) 6632.
[38] K.R. Gopidas, M. Bohorquez, P.V. Kamat, J. Phys. Chem. 94 (1990) 6435.
[39] R. Vogel, P. Hoyer, H. Weller, J. Phys. Chem. 98 (1994) 3183.
[40] P.A. Sant, P.V. Kamat, Phys. Chem. Chem. Phys. 4 (2002) 198.
[41] L.M. Peter, D.J. Riley, E.J. Tull, K.G.U. Wijayantha, Chem. Commun. (2002) 1030.
[42] N. Serpone, E. Borgarello, M. Gratzel, J. Chem. Soc. Chem. Commun. (1984) 342.
[43] A. Kumar, A.K. Jain, J. Mol. Catal. A: Chem. 165 (2001) 265.
[44] H.B. Yin, Y. Wada, T. Kitamura, T. Sakata, H. Mori, S. Yanagida, Chem. Lett. 30 (2001) 334.
[45] N. Serpone, P. Maruthamuthu, P. Pichat, E. Pelizzetti, H. Hidaka, J. Photochem. Photobiol. A: Chem. 85 (1995) 247.
[46] J.C. Yu, L. Wu, J. Lin, P.S. Li, Q. Li, Chem. Commun. (2003) 1552.
[47] H. Fujii, M. Ohtaki, K. Eguchi, H. Arai, J. Mol. Catal. A: Chem. 129 (1998) 61.
[48] M.L. Steigerwald, A.P. Alivisatos, J.M. Gibson, T.D. Harris, R. Kortan, A.J. Muller, A.M. Thayer, T.M. Duncan, D.C. Douglass, L.E. Brus, J. Am. Chem. Soc. 110 (1988) 3046.
[49] V. Arcoleo, V. Turco Liveri, Chem. Phys. Lett. 258 (1996) 223.
[50] S.Y. Chang, L. Liu, S.A. Asher, J. Am. Chem. Soc. 116 (1994) 6739.
[51] V. Chhabra, V. Pillai, B.K. Mishra, A. Morrone, D.O. Shah, Langmuir 11 (1995) 3307.
[52] J.H. Adair, T. Li, T. Kido, K. Havey, J. Moon, J. Mecholsky, A. Morrone, D.R. Talham, M.H. Ludwig, L. Wang, Mater. Sci. Eng. R. 23 (1998) 139.
[53] R.I. Walton, Chem. Soc. Rev. 31 (2002) 230.
[54] M.M. Wu, J.M. Long, A.M. Huang, Y.H. Luo, S.H. Feng, R.R. Xu, Langmuir 15 (1999) 8822.
[55] J.C. Yu, L.Z. Zhang, J.G. Yu, Chem. Mater. 14 (2002) 4647.
[56] L. Wu, J.C. Yu, X.C. Wang, L.Z. Zhang, J.G. Yu, J. Solid State Chem. 178 (2005) 321.
[57] J.F. Moulder, W.F. Stickle, P.E. Sobol, K.D. Bomben, Handbook of X-ray Photoelectron Spectroscopy, Perkin Elmer Corp. Eden Prairie, MN, 1992.
[58] N.R. Armstrong, R.K. Quinn, Surf. Sci. 67 (1977) 451.
[59] C.N. Sayers, N.R. Armstrong, Surf. Sci. 77 (1978) 301.
[60] L. Wu, J.C. Yu, L.Z. Zhang, X.C. Wang, W.K. Ho, J. Solid State Chem. 177 (2004) 2584.
[61] J.C. Yu, J.G. Yu, H.Y. Tang, L.Z. Zhang, J. Mater. Chem. 12 (2002) 81.
[62] M.Z. Rong, M.Q. Zhang, H.C. Liang, H.M. Zeng, Chem. Phys. 286 (2003) 267.
[63] C. Guillen, M.A. Martinez, C. Maffiotte, J. Herrero, J. Electrochem. Soc. 148 (2001) G602.
[64] J.C. Yu, J. Lin, D. Lo, S.K. Lam, Langmuir 16 (2000) 7304.
[65] R.F. Howe, M. Gratzel, J. Phys. Chem. 89 (1985) 4495.
[66] T. Rajh, A.E. Ostafin, O.I. Micic, D.M. Tiede, M.C. Thurnauer, J. Phys. Chem. 100 (1996) 4538.
[67] J.M. Coronado, A.J. Maira, J.C. Conesa, K.L. Yeung, V. Augugliaro, J. Soria, Langmuir 17 (2001) 5368.
[68] R.F. Howe, M. Gratzel, M. J. Phys. Chem. 91 (1987) 3906.
[69] T. Zhang, T. Oyama, A. Aoshima, H. Hidaka, J. Zhao, N. Serpone, J. Photochem. Photobiol. A: Chem. 140 (2001) 163.
[70] T. Zhang, T. Oyama, S. Horikoshi, H. Hidaka, J. Zhao, N. Serpone, Sol. Energy Mater. Sol. Cells 73 (2002) 287.
[71] I. Nakamura, N. Negishi, S. Kutsuna, T. Ihara, S. Sugihara, E. Takeuchi, J. Mol. Catal. A: Chem. 161 (2000) 205.
[72] N. Serpone, R.F. Khairutdinov, in: P.V. Kamat, D. Meisel (Eds.), Semiconductor Nanoclusters, Physical, Chemical, and Catalytic Aspects, Elsevier Science, 1997.
[73] J.P. Hoare, in: A.J. Bard, R. Parsons, J. Jordan (Eds.), Standard Potentials in Aqueous Solution, Marcel Dekker, New York, 1985.